UDC 539.4

Fatigue Assessment of Ti–6Al–4V Circular Notched Specimens Produced by Selective Laser Melting

S. M. J. Razavi,[a] P. Ferro,[b] and F. Berto[a,1]

[a] Department of Mechanical and Industrial Engineering, Norwegian University of Science and Technology (NTNU), Trondheim, Norway

[b] Department of Engineering and Management, University of Padova, Vicenza, Italy

[1] filippo.berto@ntnu.no

УДК 539.4

Утомна міцність плоских зразків із двосторонніми напівкруглими вирізами зі сплаву Ti–6Al–4V, виготовлених за технологією вибірної лазерної плавки

С. М. Дж. Разави[а], П. Ферро[б], Ф. Берто[а]

[а] Механіко-машинобудівний факультет, Норвежський університет природних і технічних наук, Тронхейм, Норвегія

[б] Факультет менеджмента та інжінірінга, Падуанський університет, Віченца, Італія

Спеціальні технології виробництва дозволяють економічно обґрунтовано виготовляти деталі складної конфігурації з мінімізацією циклу від розробки до виробництва. Для використання цієї технології до високонавантажених відповідальних елементів конструкцій необхідно вивчити специфіку її впливу на характеристики утоми отриманих матеріалів на мікро-, макро- і мезорівні. Досліджується міцність від утомленості плоских зразків (гладкі і з двосторонніми напівкруглими вирізами) зі сплаву Ti–6Al–4V, які виготовлено за технологією вибірної лазерної плавки. Для ідентифікації місця зародження тріщини від утомленості та механізму руйнування фрактограми зруйнованих зразків досліджувались методом сканувальної електронної мікроскопії. Установлено, що міцність від утомленості зразків із концентратором напружень у вигляді двосторонніх напівкруглих вирізів трохи нижча, аніж гладких зразків. Показано, що чутливість даного матеріалу до концентрації напружень дуже низька через специфіку гексагональної кристалічної решітки загартованих первинних альфа-зерен і технологічних поверхневих дефектів, характерних для вибірної лазерної плавки.

Ключові слова: спеціальні технології виробництва, напівкруглий виріз, утома, вибірна лазерна плавка.

Introduction. Additive manufacturing (AM) is a process that allows a part to be built layer-by-layer by using a combination of energy delivery and material deposition. Metallic parts are obtained starting from powders that are melted by a laser or electron beam source. This results in a high sensitivity of material properties to process parameters. According to source parameters, the material can experience different thermal histories and thus different microstructures [1–4]. The microstructure of AM parts can be highly anisotropic and can reach a density greater than 99.5% [5, 6]. For example, columnar grains are shown to grow epitaxially through the deposition layers due to cooling [5].

Compared to traditional shaping processes, AM offers different advantages such as a shorter time-to market, a near-net-shape fabrication without the need of expensive moulds and tools, a high efficiency in material utilization, the possibility to directly produce

geometries with high level of flexibility based on CAD models. On the other hand, AM parts suffer the presence of defects often related to non-optimal scan parameters (unmolten particles, spherical entrapped gas bubbles, lack of fusion) [7]. Among the AM processes, a particular attention is paid on selective laser melting (SLM), a powder bed fusion-laser (PBF-L) method [8, 9]. The possibility to create structures with complex geometries out of high performance materials has made SLM particularly interesting for aerospace and biomedical industry, where titanium alloys, and in particular Ti–6Al–4V, are widely used. Titanium alloys are in fact characterized by excellent corrosion resistance, high specific strength, low density and low elastic modulus.

Both in aerospace and biomedical applications, fatigue is the primary mechanism of rupture in components such as turbine blade, hip prosthesis and mechanical heart valve [10–12]. For this reason, the fatigue strength of additive manufactured parts is widely studied in literature. In their work about high cycle fatigue (HCF) behavior of SLM-processed Ti–6Al–4V, Leuders et al. [13] found that porosity acts as strong stress raiser and lead to failure. In order to improve the fatigue strength of titanium alloy Ti–6Al–4V manufactured by SLM, reduction of porosity was thus considered by authors much more important than microstructure optimization. In a more recent work [14], Kasperovich and Hausmann found a reduction in fatigue resistance of SLM processed TiAl6V4 compared to the wrought alloy due to a combination of the unfavourable martensitic microstructure, unmolten particles, pores, and microcracks. Finally, they found that in order to restore the fatigue resistance of the conventionally processed TiAl6V4, SLM-processed, specimens need to be subjected to hot isostatic pressing (HIP), which reduces porosity, and surface machining which reduces surface roughness. As a matter of fact, for AM parts that cannot be machined on all surfaces, the rough ‘as built’ surface should be considered as crack initiator in the fatigue design process leading to their lower fatigue strength. Finally, in that work, heat treatments were found to give no significant improvement on HCF strength.

Due to some specific design requirements such as connecting different parts together and repairing cracked or damaged structures, the majority of engineering components and structures contain notches of different shapes. By their utility, notches are prone to crack nucleation due to the intensified stress at their neighbourhood. Nucleated cracks may propagate and lead to final failure of the notched component. Hence, it is commonly attempted in design of notched components to prevent or delay the crack nucleation from the notch edge [15–19]. For this aim, failure mechanisms in presence of notches should be deeply studied.

Examination of the state-of-the-art shows that fatigue assessment and quality assurance of additively manufactured components cannot be performed accurately due to a lack of bespoke methodologies allowing the specific microstructural features as well as the specific mechanical/cracking behavior of additively manufactured materials to be modelled effectively. Therefore, owing to the growing importance of additive manufacturing technologies, fundamental theoretical understanding of fatigue properties and behavior of additively manufactured metals is a necessary step that must be taken as a matter of urgency. In this challenging scenario, the problem is complicated by the fact that, as far as components having complex geometries are concerned, no specific design criteria have been proposed so far to take into account stress concentration phenomena arising from geometrical discontinuities/features (here termed notches). Further, no fatigue data generated by testing additively manufactured notched metals can be found in the technical literature. This lack of specific knowledge makes it difficult for industry to take full advantage of the unique features of adittive manufacturing, with this preventing this powerful technology from being injected effectively into every-day manufacturing practises. In this context, this work aims to contribute to the fundamental understanding of the mechanical/cracking behavior of additively manufactured Ti–6Al–4V specimens weakened by circular notches and subjected to fatigue loading.

1. **Material**, **Geometries**, **and Experimental Procedure**. The analyzed Ti–6Al–4V specimens were produced by means of SLM by using optimized process parameters that guaranteed a density greater than 99.7%. After specimens' production, specimens were sandblasted at 6 bar using corundum sand with a mean grain size of 220 μm. They were then stress relief heat-treated in non-controlled atmosphere (heating rate: 10.8 ℃/min; holding time: 3h at 650℃; cooling rate: 2 ℃/min) and after cutting off the base plate they were re-sandblasted at 6 bar using corundum sand. All specimens were obtained by using a layer thickness of 60 μm. Figure 1 shows the geometries of smooth and circular notched specimens. The radius at the notch is 5 mm while the thickness of the specimens is 3 mm.

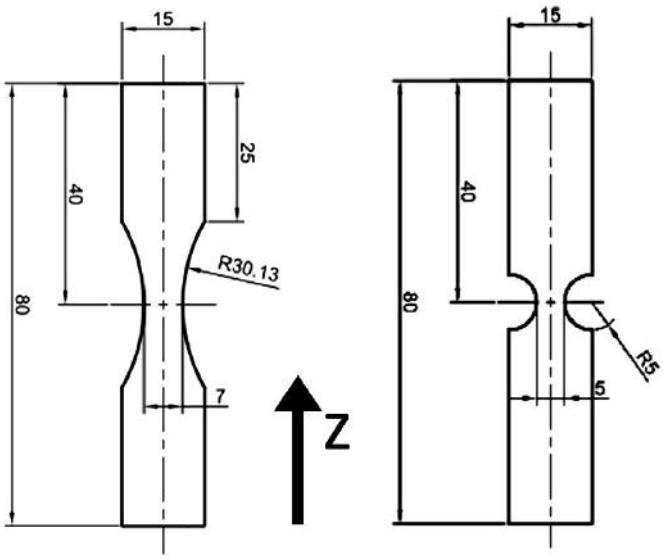

Fig. 1. Geometries of smooth and circular notched specimens and built axis (*Z*) (dimensions in mm).

Fatigue tests were carried out by using a universal MTS machine (250 kN). All tests have been carried out under load control, using a sinusoidal signal in uniaxial tension with a frequency of 10 Hz and load ratio $R = 0$. The run out limit was set equal to 10^6 cycles. The microstructure and the fracture surface of the specimens were investigated by optical microscope (OM) and environmental scanning electron microscope (ESEM) (FEI QUANTA 400), respectively.

Kroll's Reagent (2 ml HF, 2 ml HNO_3, 100 ml H_2O) was used as metallographic etchant. The alpha prime and acicular alpha structures of titanium alloy will appear white after etching while intergranular beta structure and beta grains will be darkened.

A numerical model under plain stress condition was carried out using ANSYS® numerical code, in order to calculate the stress concentration factor, K_t. The Young modulus and Poisson's ratio were set equal to 110 GPa and 0.34, respectively. By taking advantage of the double symmetry, only one fourth of the specimen was modelled by using a mapped mesh (Fig. 2a). Figure 2b shows the principal stress distribution induced by a remotely applied tension (σ_n) of 213 MPa.

2. **Results**.

2.1. ***Fatigue Test Results***. Results obtained from the statistical elaboration of fatigue tests data for smooth and notched specimens are reported in Figs. 3 and 4, respectively. Values of stress amplitude related to a survival probability of 50%, the slope of the Wöhler curve and the scatter index T_σ (the ratio between the stress amplitudes corresponding to 10 and 90% of survival probability) are reported in the above figures. Specimens survived

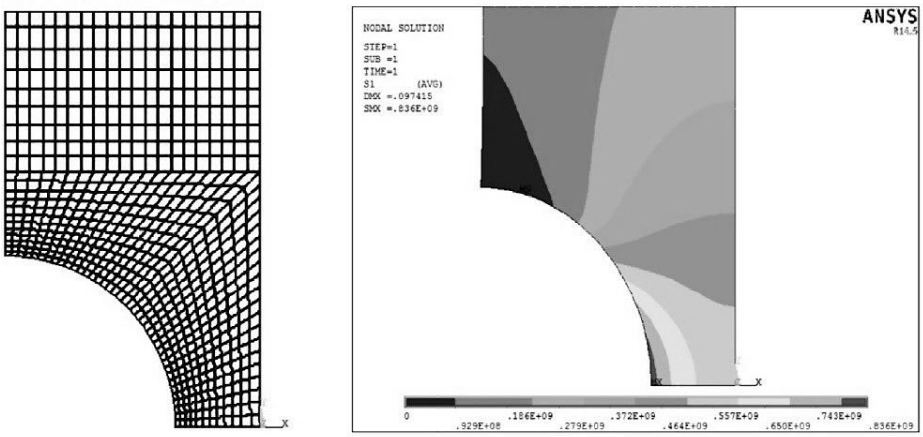

a b

Fig. 2. Mesh of the specimen with a double circular notch (a) and principal stress (S_1) distribution induced by a remotely applied tension (σ_n) of 213 MPa.

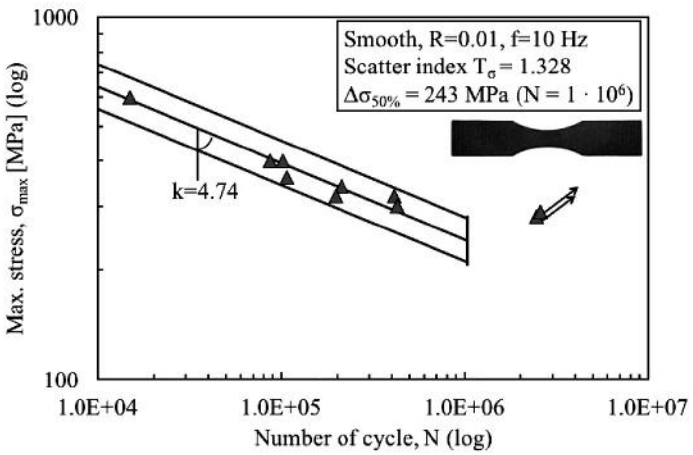

Fig. 3. Fatigue curve of Ti–6Al–4V smooth specimens.

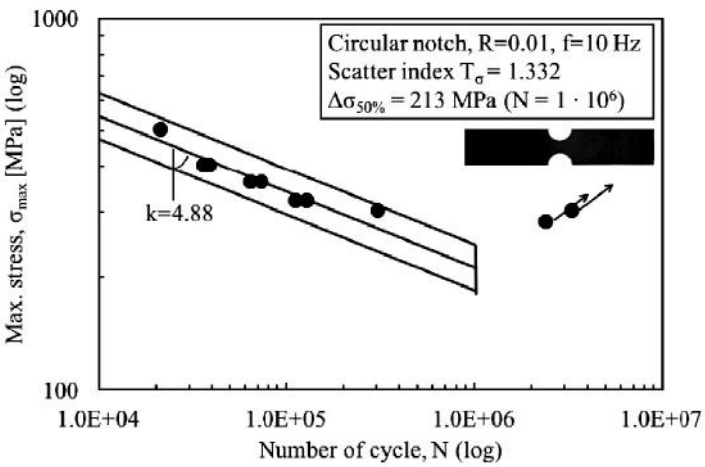

Fig. 4. *S–N* curve of Ti–6Al–4V double blunt V-nothced specimens.

over 1 million cycles are considered as run out and marked up with an arrow. It can be noted that the difference between the Wohler curves are related only to the mean value of the stress amplitude at $1 \cdot 10^6$ cycles, but not to the scatter index T_σ. The fatigue strength of double circular notched specimens at 1 million cycles was 213 MPa compared to a value of 243 MPa related to the fatigue strength of smooth samples

2.2. ***Microstructure and Fractography***. A preliminary microstructure investigation by means of OM showed an almost porosity-free material. Some occasional porosity was found which dimension was less than 50 μm. OM and ESEM micrographs are shown in Fig. 5. The grains appear acicular with a prevalence of α' plates surrounded by a little percentage of β phase. In Fig. 5a the primary equiassic morphology of β phase prior to the $\beta \to \alpha'$ transformation can be also observed. In Fig. 5b the Al-reach black zones correspond to α' phase, tempered by stress-relief heat treatment, while the white zones, reach in vanadium, correspond to β phase. Such a microstructure is due to the high cooling rate that characterizes the SLM process and the subsequent heat treatment below 800℃.

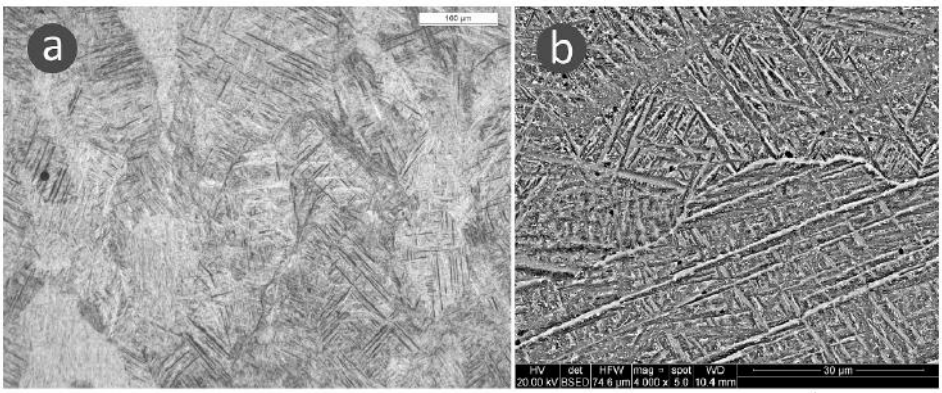

Fig. 5. Optical microscope (a) and environmental scanning electron microscope (b) micrographs of the analyses material.

ESEM fractographs of the smooth and blunt circular notched specimens are shown in Figs. 6 and 7, respectively. It is noted that fatigue cracks nucleate at the specimen surface both in smooth and double U-notched specimens where severe intrusions (Fig. 6d), due to the roughness induced by the process, act as crack initiation points (Figs. 6d and 7). The fracture nucleates at one point at the surface of the smooth specimen (Fig. 6d) and propagates towards the opposite edge covering almost the entire cross section of the specimen until the final rupture. The final fracture surface, characterized by dimples (Fig. 6c), was found to be inclined by about 45° with respect to the load direction (Fig 6a). No porosity was observed on fracture surface of all specimens. In a similar way, fatigue cracks nucleate at both the notch tip of the double circular notched specimen. Thus, the final fracture surface appears in between the two propagation zones and still inclined by about 45° with respect to the load direction. Figure 7 shows a typical deep intrusion where a crack nucleated.

Finally, despite the several detected high intrusions at the surface that act as easy crack nucleation zones, it was found that fatigue cycles spent for crack nucleation were much higher than those spent for crack propagation (Fig. 8).

In Fig. 8 the stiffness of both a smooth and a circular notched specimen loaded with the same remotely applied stress ($\sigma_n = 360$ MPa) was plotted against the cycles number. It is noted that the stiffness of both specimens remains constant for about 90% of the fatigue life. In particular, the crack nucleation period was set equal to the number of cycles beyond which all the experimental points fall down under the interpolation straight line shown in

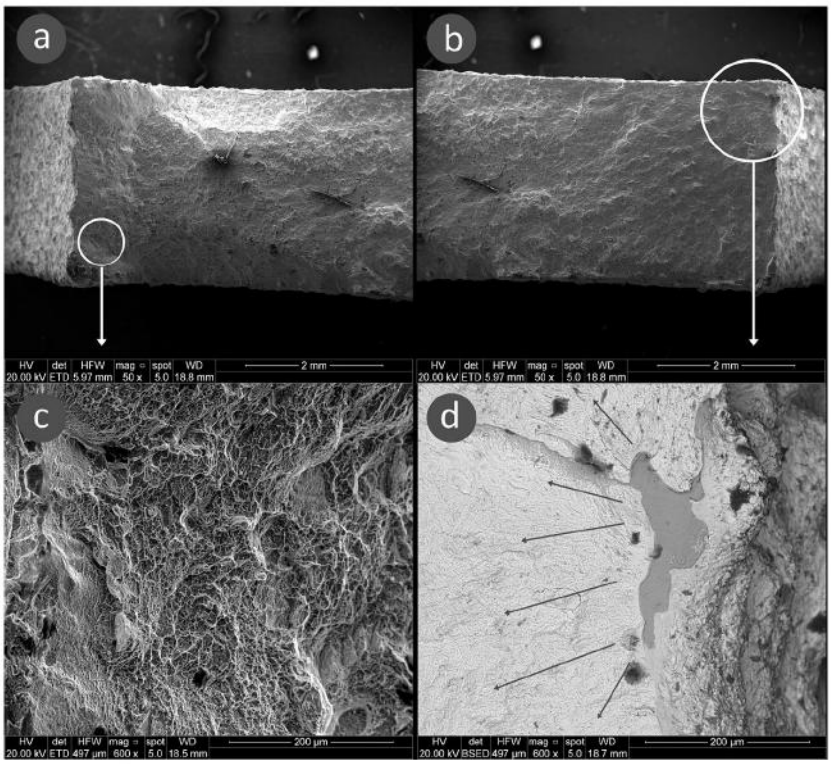

Fig. 6. ESEM fractographs of the smooth specimen ($\Delta\sigma = 360$ MPa, $N = 106{,}374$ cycles).

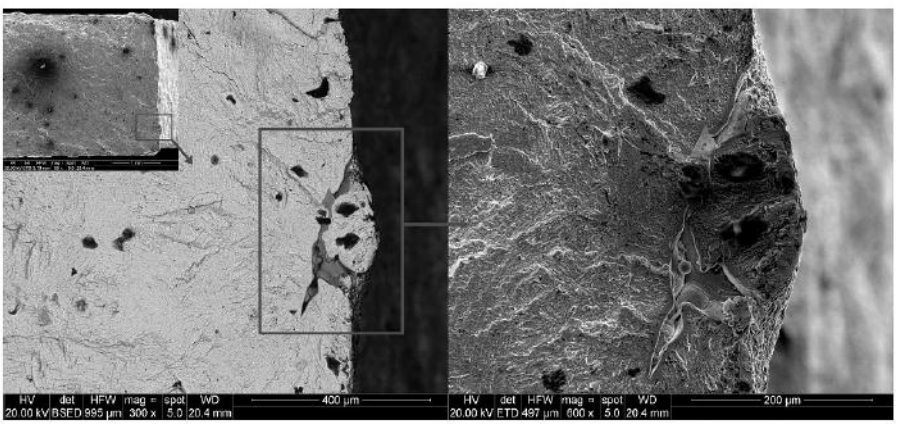

Fig. 7. ESEM fractographs of the double circular notched specimen ($\Delta\sigma = 360$ MPa, $N = 64{,}427$ cycles).

Fig. 8. By analyzing all specimens with this procedure, it was found that the percentages of fatigue life spent for crack nucleation were 93 and 81% for smooth and circular notched specimen, respectively.

3. **Discussion**. By using the obtained experimental data, the notch sensitivity has been calculated. The notch sensitivity (q) is defined by Eq. (1):

$$q = \frac{K_f - 1}{K_t - 1}, \tag{1}$$

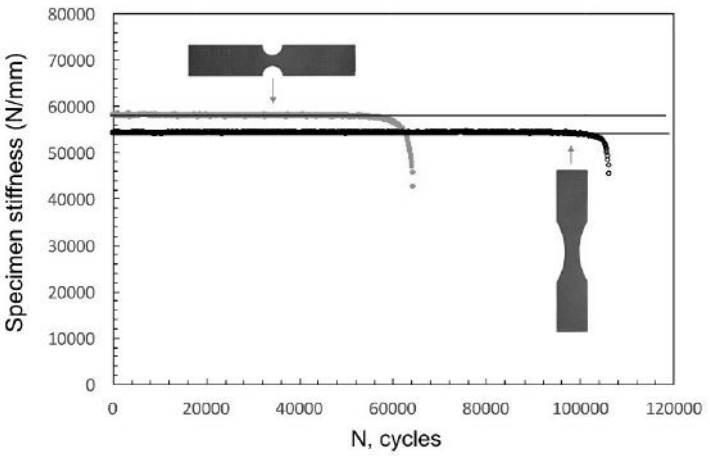

Fig. 8. Specimen stiffness as a function of cycles number of a smooth and a circular notched specimen, both loaded with a nominal stress (σ_n) value of 360 MPa.

where K_f is the fatigue notch factor ($K_f = \Delta\sigma_A^{smooth} / \Delta\sigma_A^{V-nothc}$) and K_t is the stress concentration factor defined by maximum local stress to nominal stress ratio ($K_t = \sigma_{\max} / \sigma_{nom}$) [20]. The nominal stress is defined as the mean stress across the reduced cross-section of the specimen in the presence of the notch. In general, $0 \le q \le 1$. When the theoretical stress concentration factor equals the fatigue notch factor (i.e., $K_f = K_t$), $q = 1$. If the notch has no adverse effect on the fatigue limit (i.e., $K_f = 1$), $q = 0$. By using the fatigue data obtained in this work, $K_f = 1.141$. K_t was found equal to 3.925 by a numerical simulation. This results in a q value equal to 0.048.

A low notch sensitivity of the wrought Ti–6Al–4V alloy was already observed by Hosseini [20]. She justified such alloy behavior through alpha hexagonal close packed (hcp) crystal lattice characteristics. Compared to cubic lattices, such as face central cubic (fcc) or body central cubic (bcc) lattice, the slip planes in hcp lattice are all parallel to each other (planes (0001) in Miller–Bravais system). The slip systems number for dislocations in a hcp lattice are thus very low if compared to those in a cubic crystal (CC). Now, dislocations play a key role in the fatigue crack nucleation phase. It has been revealed that after a large number of fatigue loading cycles, dislocations pile up and form structures called persistent slip bands (PSB). Such PSB can be formed more easily in a crystal grain that has an unfavourable orientation of its slip planes relative to the planes of maximum applied shear stresses (Fig. 9). Because of its few slip systems, for a hcp lattice, such unfavourable orientations are very few. In this situation, many potential damage initiation sites occur within the volume of a smooth specimen but, at the sharp notch, it is possible that almost no damage initiation site occurs in the small region around the notch tip where the stress is near its peak value. Hence, considering the local notch stress, the notched member can be more resistant to fatigue.

As shown in Figs. 6 and 7, fatigue cracks were observed to initiate on severe surface intrusions due to the high roughness induced by the process itself. Such intrusions are covered by an oxide layer which was formed during the stress-relief heat treatment and non-cleaned up by the grinding treatment. Now, the number of potential crack initiation intrusions is thought to be much higher in smooth specimens than in the sharp V-notch specimen where there is the possibility that no such critical surface defects occur in the small region near the notch tip. It is thought that this effect and the alpha prime hcp lattice characteristics may justify the very low notch sensitivity of the SLM-processed Ti–6Al–4V alloy observed by experiments.

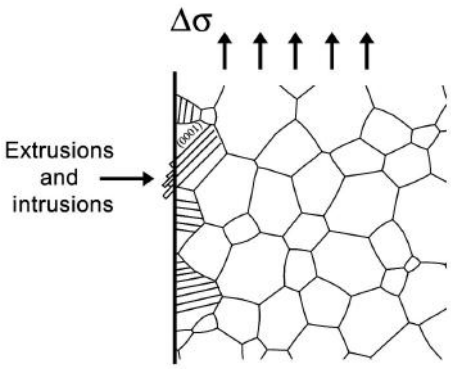

Fig. 9. Schematic representation of PSB formed in a crystal grain that has an unfavourable orientation of its (0001) slip planes relative to the planes of maximum applied shear stresses.

In order to better comprehend the mechanism of crack nucleation in alpha phase, the fatigue test of a specimen with double circular notch was interrupted when its stiffness values started to fall down. The resulting fatigue cracks were then observed by means of electron backscattered diffraction (EBSD) technique. Figure 10 shows SEM and EBSD micrographs of a fatigue crack and corresponding alpha grains orientation at the initiation and propagation zones. It is observed how the basal slip planes of the alpha grain at the crack initiation zone are oriented about 45° compared to the load direction.

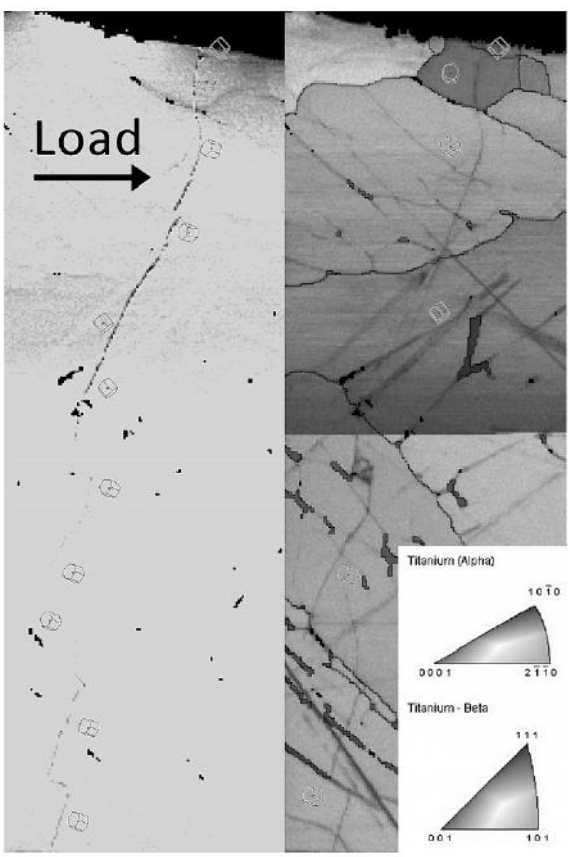

Fig. 10. SEM and EBSD micrograph of a fatigue crack in a circular notched specimen.

Conclusions. The fatigue strength of Ti–6Al–4V circular notched specimens produced by SLM was assessed. Results were compared with those corresponding to smooth specimens and scanning electron microscopy have been used to investigate the fracture surface of broken specimens in order to identify crack initiation points and fracture mechanisms. Despite the fatigue specimens were weakened by the sharp circular notch, a very low notch sensitivity was measured. This was attributed both to the hexagonal crystal lattice of tempered alpha prime grains and to the high roughness detected on specimen surface.

Р е з ю м е

Специальные технологии производства позволяют экономически обосновано изготовлять детали сложной конфигурации с минимизацией цикла от разработки до производства. Для применения этой технологии к высоконагруженным ответственным элементам конструкций необходимо изучить специфику ее влияния на характеристики усталости полученных материалов на микро-, макро- и мезоуровне. Исследуется усталостная прочность плоских образцов (гладкие и с двухсторонними полукруглыми вырезами) из сплава Ti–6Al–4V, изготовленных по технологии избирательной лазерной плавки. Для идентификации мест зарождения усталостной трещины и механизма разрушения фрактограммы разрушенных образцов исследовались методом сканирующей электронной микроскопии. Установлено, что усталостная прочность образцов с концентратором напряжений в виде двухсторонних полукруглых вырезов незначительно ниже, чем гладких образцов. Показано, что чувствительность данного материала к концентрации напряжений очень низкая из-за специфики гексагональной кристаллической решетки закаленных первичных альфа-зерен и технологических поверхностных дефектов, характерных для избирательной лазерной плавки.

1. M. Todai, T. Nakano, T. Liu, et al., “Effect of building direction on the microstructure and tensile properties of Ti-48Al-2Cr-2Nb alloy additively manufactured by electron beam melting,” *Addit. Manuf.*, **13**, 61–70 (2017).
2. A. Domashenkov, A. Plotnikova, I. Movchan, et al., “Microstructure and physical properties of a Ni/Fe-based superalloy processed by Selective Laser Melting,” *Addit. Manuf.*, **15**, 66–77 (2017).
3. Y. S. Lee and W. Zhang, “Modeling of heat transfer, fluid flow and solidification microstructure of nickel-base superalloy fabricated by laser powder bed fusion,” *Addit. Manuf.*, **12**, Part B, 178–188 (2016).
4. L. E. Lindgren, A. Lundbäck, M. Fisk, et al., “Simulation of additive manufacturing using coupled constitutive and microstructure models,” *Addit. Manuf.*, **12**, Part B, 144–158 (2016).
5. X. Wu, J. Liang, J. Mei, et al., “Microstructures of laser-deposited Ti–6Al–4V,” *Mater. Design*, **25**, No. 2, 137–144 (2014).
6. E. Wycisk, S. Siddique, D. Herzog, et al., “Fatigue performance of laser additive manufactured Ti–6A–4V in very high cycle fatigue regime up to 10^9 cycles,” *Front. Mater.*, **2** (2015), DOI: 10.3389/fmats.2015.00072.
7. T. Vilaro, C. Colin, and J. D. Bartout, “As-fabricated and heat-treated microstructures of the Ti-6Al-4V alloy processed by selective laser melting,” *Metall. Mater. Trans. A*, **42**, No. 10, 3190–3199 (2011).
8. J. P. Kruth, P. Mercelis, J. Van Vaerenbergh, et al., “Binding mechanism in selective laser sintering and selective laser melting,” *Rapid Prototyp. J.*, **11**, No. 1, 26–36 (2005).

9. B. Vrancken, L. Thijs, J. P. Kruth, and J. V. Humbeeck, "Heat treatment of T6Al4V produced by selective laser melting: microstructure and mechanical properties," *J. Alloy. Compd.*, **541**, 177–185 (2012).
10. N. E. Cherolis, "Fatigue in the aerospace industry: Striations," *J. Fail. Anal. Preven.*, **8**, No. 3, 255–258 (2008).
11. X. Song, L. Wang, M. Niinomi, et al., "Microstructure and fatigue behaviors of a biomedical Ti–Nb–Ta–Zr alloy with trace CeO_2 additions," *Mater. Sci. Eng. A*, **619**, 112–118 (2014).
12. Z. Sun, M. Chemkhi, P. Kanoute, and D. Retraint, "Fatigue properties of a biomedical 316L steel processed by surface mechanical attrition," *IOP Conf. Ser.: Mater. Sci. Eng.*, **63**, 012021 (2014), DOI: 10.1088/1757-899X/63/1/012021.
13. S. Leuders, M. Thöne, A. Riemer, et al., "On the mechanical behaviour of titanium alloy TiAl6V4 manufactured by selective laser melting: fatigue resistance and crack growth performance," *Int. J. Fatigue*, **48**, 300–307 (2013).
14. G. Kasperovich and J. Hausmann, "Improvement of fatigue resistance and ductility of TiAl6V4 processed by selective laser melting," *J. Mater. Process. Tech.*, **220**, 202–214 (2015).
15. F. Berto and E. Barati, "Fracture assessment of U-notches under three point bending by means of local energy density," *Mater. Design*, **32**, No. 2, 822–830 (2011).
16. F. Berto, P. Lazzarin, and M. R. Ayatollahi, "Brittle fracture of sharp and blunt V-notches in isostatic graphite under pure compression loading," *Carbon*, **63**, 101–116 (2013).
17. F. Berto, P. Lazzarin, and C. Marangon, "Fatigue strength of notched specimens made of 40CrMoV13. 9 under multiaxial loading," *Mater. Design*, **54**, 57–66 (2014).
18. S. M. J. Razavi, M. R. Ayatollahi, C. Sommitsch, and C. Moser, "Retardation of fatigue crack growth in high strength steel S690 using a modified stop-hole technique," *Eng. Fract. Mech*., **169**, 226–237 (2017).
19. M. R. Ayatollahi, S. M. J. Razavi, C. Sommitsch, and C. Moser, "Fatigue life extension by crack repair using double stop-hole technique," *Mater. Sci. Forum*, **879**, 3–8 (2017).
20. S. Hosseini, "Fatigue of Ti-6Al-4V," in: R. Hudak, M. Penhaker, and J. Majernik (Eds.), *Biomedical Engineering – Technical Applications in Medicine*, Ch. 3, InTech, Rijeka (2012), pp. 75–92, ISBN 978-953-51-0733-0.

Received 12. 12. 2016